New Trigonal-Bipyramidal 5-*ansa*-Zirconocene Derivatives. 1. {2,6-Bis(methylcyclopentadienyl)-pyridine}zirconium(IV) Monochloride Monoalkyls and Dialkyls. Crystal Structure of $[Zr\{C_5H_3N(CH_2C_5H_4)_2\text{-}2,6\}(n\text{-}C_4H_9)_2]$, the First Thermally Stable Dialkylzirconocene Containing β-Hydrogens

Gino Paolucci,*[,†] Giulio Pojana,[†] Jacopo Zanon,[†] Vittorio Lucchini,*[,‡] and Evgeni Avtomonov[§]

Dipartimento di Chimica and Dipartimento di Scienze Ambientali, Università di Venezia, Calle Larga S. Marta 2137, I-30123 Venezia, Italy, and Department of Chemistry, Philipps Universität Marburg, Hans-Meerwein-Strasse, D-35032 Marburg, Germany

Received April 14, 1997[⊗]

The reaction of the new ligand $[2,6\text{-}(CH_2C_5H_4)_2C_5H_3N]^{2-}Na^+_2$ (LNa_2) with $ZrCl_4$ in THF affords in good yield the trigonal-bipyramidal complex $LZrCl_2$, where the two chlorine atoms are not equivalent. When $LZrCl_2$ and RMgCl (R = CH_3, *n*-butyl, $CH_2Si(CH_3)_3$) are reacted in 1:1 and 1:2 molar ratios, the corresponding complexes LZr(Cl)R and $LZrR_2$ can be isolated in good yields. Differently from the $Cp_2Zr(n\text{-}Bu)_2$, which has never been isolated due to β-H elimination, the analogous $LZr(n\text{-}Bu)_2$ is thermally stable and its X-ray crystal structure has been solved, confirming its trigonal-bipyramidal geometry with the alkyl groups occupying an equatorial and an axial position. An NMR study (^1H, ^{13}C, HMQC, NOE) allowed the complete structural characterization of the complexes in solution.

Introduction

After the discovery of the zirconocene−methylalumoxane (Zr-MAO) systems as powerful catalysts for the isotactic[1] and syndiotactic[2] polymerization of propylene, a great deal of scientific work on the explanation of the factors affecting the stereospecificity[3−15] and on the relationship between the structures of these systems and the chain growth of the polymer[16] has been promoted worldwide. With the aim of realizing high activity and stereoselectivity of the catalysts and of yielding high-molecular-weight polymers, a number of new *ansa*-zirconocenes have been synthesized.[17−24]

Most synthesized zirconocenes have a pseudotetrahedral geometry, and all efforts to increase their stereoselectivity have been directed in increasing the steric hindrance around the zirconium ion by adding sterically demanding substituents to the ligands. In fact, it is generally accepted that the steric environment around the metal directs the orientation of the approaching monomer, thus ultimately improving the tacticity.[25]

A key feature of the $[Cp_2Zr(R)]^+$ d^0 species is represented by the Cp_2Zr framework that forces the vacant coordination sites to be oriented *cis* to the Zr−R bond and can be extensively modified by substitution in order to tune steric and electronic properties. The synthesis of *ansa*-zirconocenes with trigonal-bipyramidal geometries could, in principle, require less sterically demanding substituents to obtain the desired stereoselectivity. Recently, we reported the synthesis of new complexes of the type $LUCl_2$[26] and $[LLnCl]_2$[27] (L = 2,6-

† Dipartimento di Chimica, Università di Venezia.
‡ Dipartimento di Scienze Ambientali, Università di Venezia.
§ Philipps Universität Marburg.
⊗ Abstract published in *Advance ACS Abstracts,* August 15, 1997.

(1) Kaminsky, W.; Kulper, K.; Brintzinger, H. H.; Wild, F. R. W. P. *Angew. Chem., Int. Ed. Engl.* **1985**, *24*, 507.
(2) Ewen, J. A.; Jones, R. L.; Razavi, A. *J. Am. Chem. Soc.* **1988**, *110*, 6255.
(3) Ewen, J. A. In *Catalytic Polymerisation of Olefins*; Keii, T., Soga, K., Eds.; Kohdansha Elsevier: Tokyo, 1986; p 271.
(4) Ewen, J. A.; Haspeslagh, L.; Elder, M. J.; Atwood, J. L.; Zhang, H.; Cheng, H. N. In *Transition Metals as Catalysts for Olefin Polymerisation*; Kaminsky, W., Sinn, H., Eds.; Springer: Berlin, 1988; p 281.
(5) Mise, T.; Miya, S.; Yamazaki, H. *Chem. Lett.* **1989**, 1853.
(6) Herrmann, W. A.; Rohrmann, J.; Herdtweck, E.; Spaleck, W.; Winter, A. *Angew. Chem.* **1989**, *101*, 1536.
(7) Spaleck, W.; Antberg, M.; Dolle, V.; Klein, R.; Rohrmann, J.; Winter, A. *New J. Chem.* **1990**, *14*, 499.
(8) Roll, W.; Brintzinger, H. H.; Rieger, B.; Zolk, R. *Angew. Chem., Int. Ed. Engl.* **1990**, *29*, 279.
(9) Collins, S.; Gathier, W. J.; Holden, D. A.; Kuntz, B. A.; Taylor, N. J.; Ward, D. G. *Organometallics* **1991**, *10*, 2061.
(10) Gavallo, L.; Guerra, G.; Vacatello, M.; Corradini, P.; *Macromolecules* **1991**, *24*, 1784.
(11) Longo, P.; Proto, A.; Grassi, A.; Ammendola, P. *Macromolecules* **1991**, *24*, 4624.
(12) Brintzinger, H. H. In *Organic Synthesis via Organometallics*; Dotz, K. H., Hoffmann, R. W., Eds.; Vieweg: Braunschweig, Germany, 1991; p 33.
(13) Hortmann, K.; Brintzinger, H. H. *New J. Chem.* **1992**, *16*, 51.
(14) Burger, P.; Oiebold, J.; Gutmann, S.; Hund, H.-U.; Brintzinger, H. H. *Organometallics* **1992**, *11*, 1319.
(15) Lee, I.-M.; Gauthier, W. J.; Ball, J. M.; Iyengar, B.; Collins, S. *Organometallics* **1992**, *11*, 2115.
(16) Pino, P.; Cioni, P.; Wei, J. *J. Am. Chem. Soc.* **1987**, *91*, 613.
(17) Davis, B. R.; Bernal, I. *J. Organomet. Chem.* **1971**, *30*, 75.
(18) Epstein, E. F.; Bernal, I. *Inorg. Chim. Acta* **1973**, *7*, 211.
(19) Curtis, M. D.; D'Errico, J. J.; Duffy, D. N.; Epstein, P. S.; Bell, L. G. *Organometallics* **1983**, *2*, 1808.
(20) Roll, W.; Zsolnai, L.; Huttner, G.; Brintzinger, H. H. *J. Organomet. Chem.* **1987**, *322*, 65.
(21) Lang, H.; Seyferth, D. *Organometallics* **1991**, *10*, 347.
(22) Qian, C.; Guo, J.; Ye, C.; Sun, J.; Zheng, P. *J. Chem. Soc., Dalton Trans.* **1993**, 3441.
(23) Rieger, B.; Jany, G.; Fawzi, R.; Steimann, M. *Organometallics* **1994**, *13*, 647.
(24) Gräper, J.; Paolucci, G.; Fischer, R. D. *J. Organomet. Chem.* **1995**, *501*, 211.
(25) Hart, J. R.; Rappé, A. K. *J. Am. Chem. Soc.* **1993**, *115*, 6159 and references therein.
(26) Paolucci, G.; Fischer, R. D.; Benetollo, F.; Seraglia, R.; Bombieri, G. *J. Organomet. Chem.* **1991**, *412*, 327.

S0276-7333(97)00311-7 CCC: $14.00

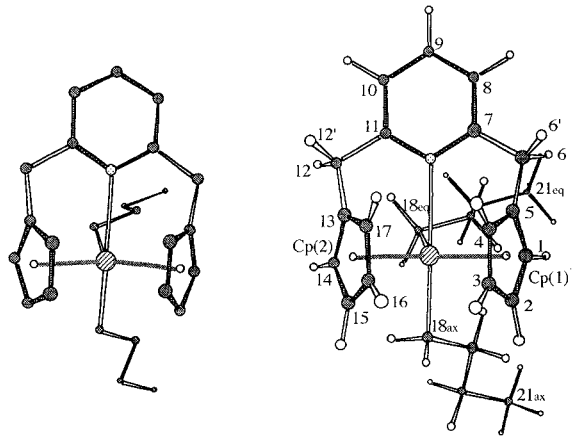

LZr(*n*-Bu)$_2$, X-ray structure LZr(*n*-Bu)$_2$, computed structure

N-Zr	2.531 Å	2.497 Å
Zr-C(18)$_{ax}$	2.355 Å	2.344 Å
Zr-C(18)$_{eq}$	2.385 Å	2.338 Å
Zr-Cp(1)	2.235 Å	2.281 Å
Zr-Cp(2)	2.230 Å	2.280 Å
N-Zr-C(18)$_{ax}$	210.7°	205.4°
N-Zr-C(18)$_{eq}$	70.8°	73.3°
N-Zr-Cp(1)	91.5°	91.4°
N-Zr-Cp(2)	93.0°	91.4°
C(18)$_{eq}$-Zr-C(18)$_{ax}$	78.7°	81.4°
C(18)$_{ax}$-Zr-Cp(1)	101.0°	102.0°
C(18)$_{ax}$-Zr-Cp(2)	99.4°	97.3 °
C(18)$_{eq}$-Zr-Cp(1)	119.3°	125.0 °
C(18)$_{eq}$-Zr-Cp(2)	108.3°	106.7°
Cp(1)-Zr-Cp(2)	130.8°	126.7°

Figure 1. Comparison of the computed and X-ray crystal structures of LZr(*n*-Bu)$_2$ (**2**). Cp(1) and Cp(2) represent the cyclopentadienyl centroids.

$(CH_2C_5H_4)_2C_5H_3N$), where the ligand induces unusual trigonal-bipyramidal geometries. The X-ray crystal structure of the compound $LUCl_2$ showed that the two chlorine atoms are not equivalent, having distinct equatorial and axial orientations.[26] On the other hand, $LZrCl_2$ has been characterized by ^{1}H NMR, IR, MS, and XPS as a pentacoordinated complex,[22] while the X-ray analysis of $[LZr(Cl)H_2O]_2[ZrCl_6]$ shows a trigonal-bipyramidal geometry with the chlorine atom and the water molecule in equatorial and axial orientations, respectively.[28]

Unlike the alkylchlorozirconocenes, which are thermally stable at room temperature, dialkylzirconocenes containing one or more β C−H bonds are thermally labile.[29−31]

We report herein the synthesis of trigonal-bipyramidal monoalkyl- and dialkylzirconium(IV) derivatives obtained by the stepwise reaction of $LZrCl_2$ with either lithium alkyls or Grignard reagents. A complete NMR study (^{1}H, ^{13}C, HMQC, NOEDS) allowed the structural determination of all complexes in solution. The determination was facilitated by a comparison with ab initio optimized structures.[32] The structure of the surprisingly stable $LZrR_2$ (R = *n*-Bu) has also been determined in the solid state by X-ray analysis at −100 °C.

Table 1. Absolute Energies (3-21G*//PM3) and Relative Energies of *ansa*-Zirconocenes 1−7

compd	abs energy (hartree)	relative energy (kcal mol^{-1})
$LZrCl_2$ (**1**)	−5 140.239 933 3	
LZr(*n*-Bu)$_2$ (**2**)	−4 536.928 860 5	
$LZrMe_2$ (**3**)	−4 304.056 129 6	
$LZr(CH_2SiMe_3)_2$ (**4**)	−5 114.358 561 5	
LZr(*n*-Bu)$_{ax}$Cl$_{eq}$ (**5a**)	−4 838.593 915 1	0
LZr(*n*-Bu)$_{eq}$Cl$_{ax}$ (**5b**)	−4 838.585 535 3	5.26
LZr(Me)$_{ax}$Cl$_{eq}$ (**6a**)	−4 722.155 449 7	0
LZr(Me)$_{eq}$Cl$_{ax}$ (**6b**)	−4 722.147 936 6	4.71
$LZr(CH_2SiMe_3)_{ax}Cl_{eq}$ (**7a**)	−5 127.306 708 7	0
$LZr(CH_2SiMe_3)_{eq}Cl_{ax}$ (**7b**)	−5 127.302 473 9	2.66

Results

As previously reported,[22] the reaction in THF of the disodium salt of the ligand LNa_2 with $ZrCl_4$ affords the corresponding monomeric unsolvated complex $LZrCl_2$ (**1**). A careful NMR analysis of the complex, detailed in the next section, shows that the two chlorine atoms are nonequivalent and therefore possess distinct axial and equatorial orientations. This feature has been confirmed by ab initio computations.[32] When **1** is reacted with RMgCl or RLi in a 1:2 molar ratio in THF at −80 °C, the corresponding dialkyl derivatives (**2**−**4**) are obtained in good yields (eq 1).

$$\underset{\mathbf{1}}{LZrCl_2} + 2RM \rightarrow \underset{\begin{array}{l}\mathbf{2}:\ R = n\text{-Bu}\\ \mathbf{3}:\ R = Me\\ \mathbf{4}:\ R = CH_2SiMe_3\end{array}}{LZrR_2} + \underset{\begin{array}{l}M = Li, MgCl\\ M = Li\\ M = Li, MgCl\end{array}}{2MCl} \quad (1)$$

At variance with the fact that "$Cp_2Zr(n\text{-Bu})_2$" has never been isolated because of the β-H elimination reaction of the two *n*-butyl groups,[31] the complex **2** shows an unusually high thermal stability. It melts without decomposition at 105 °C and decomposes at about 140−150 °C.

When the same reactions are carried out in a 1:1 molar ratio, the corresponding chloroalkyl derivatives (**5**−**7**) can be obtained in good yields (eq 2). All

$$\underset{\mathbf{1}}{LZrCl_2} + RM \rightarrow \underset{\begin{array}{l}\mathbf{5}:\ R = n\text{-Bu}\\ \mathbf{6}:\ R = Me\\ \mathbf{7}:\ R = CH_2SiMe_3\end{array}}{LZrRCl} + \underset{\begin{array}{l}M = Li, MgCl\\ M = Li\\ M = Li, MgCl\end{array}}{MCl} \quad (2)$$

complexes have been characterized as monomeric and unsolvated compounds by elemental analysis, MS spectrometry and ^{1}H and ^{13}C NMR spectroscopy.

Computational Optimization of *ansa*-Zirconocenes 1−7 and X-ray Crystal Structure of LZr(*n*-Bu)$_2$ (2). The geometries of complexes **1**−**7** have been optimized at the semiempirical PM3 level. The energies of the optimized structures have been recomputed at the ab initio 3-21G* level. The results are summarized in Table 1. The discussion will refer to the numbering given in Figure 1. For the sake of simplicity, equivalent protons will be referenced with the lower

(27) Paolucci, G.; D'Ippolito, R.; Ye, C.; Qian, C.; Gräper, J.; Fischer, R. D. *J. Organomet. Chem.* **1994**, *471*, 97.
(28) Thiele, K. H.; Schlessburg, Ch.; Neumüller, B. *Z. Anorg. Allg. Chem.* **1995**, *621*, 1106.
(29) Negishi, E.; Swanson, D. R.; Takahashi, T. *J. Chem. Soc., Chem. Commun.* **1990**, 1254.
(30) Negishi, E.; Nguyen, T.; Maye, J. P.; Choueiri, D.; Suzuki, N.; Takahashi, T. *Chem. Lett.* **1992**, 2367.
(31) Negishi, E.; Takahashi, T. *Acc. Chem. Res.* **1994**, *27*, 124.
(32) SPARTAN version 4.0: distributed by Wavefunction, Inc., 18401 Von Karman Ave., Irvine, CA 92715.

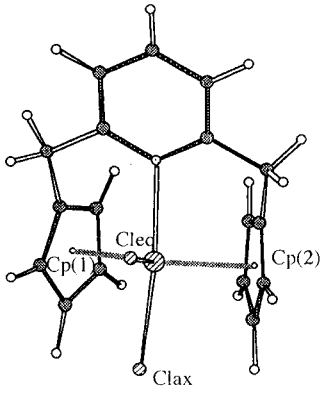

$LZrCl_2$ (**1**)

Zr-N	2.404Å	N-Zr-Cl_{ax}	212.7°
Zr-Cl_{ax}	2.510Å	N-Zr-Cl_{eq}	70.4°
Zr-Cl_{eq}	2.485Å	N-Zr-Cp(1)	95.1°
Zr-Cp(1)	2.232Å	N-Zr-Cp(2)	95.1°
Zr-Cp(2)	2.232Å	Cl_{ax}-Zr-Cl_{eq}	77.0°
		Cl_{ax}-Zr-Cp(1)	97.7°
		Cl_{ax}-Zr-Cp(2)	97.7°
		Cl_{eq}-Zr-Cp(1)	113.1°
		Cl_{ax}-Zr-Cp(2)	113.2°
		Cp(1)-Zr-Cp(2)	133.3°

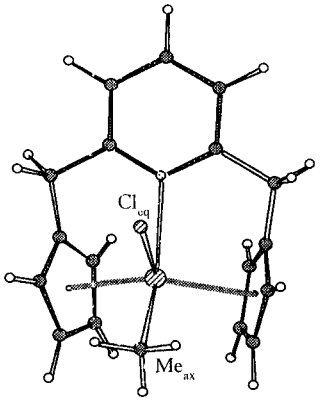

$LZrMe_{ax}Cl_{eq}$ (**6a**)

Zr-N	2.414Å	N-Zr-Me_{ax}	217.7°
Zr-Cl_{eq}	2.524Å	N-Zr-Cl_{eq}	68.6°
Zr-Me_{ax}	2.485Å	N-Zr-Cp(1)	95.3°
Zr-Cp(1)	2.237Å	N-Zr-Cp(2)	95.2°
Zr-Cp(2)	2.237Å	Me_{ax}-Zr-Cl_{eq}	73.8°
		Me_{ax}-Zr-Cp(1)	99.6°
		Me_{ax}-Zr-Cp(2)	99.6°
		Cl_{eq}-Zr-Cp(1)	113.4°
		Cl_{eq}-Zr-Cp(2)	132.6°
		Cp(1)-Zr-Cp(2)	132.6°

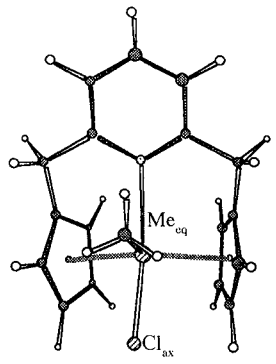

$LZrMe_{eq}Cl_{ax}$ (**6b**)

Zr-N	2.400Å	N-Zr-Cl_{ax}	210.1°
Zr-Cl_{ax}	2.526Å	N-Zr-Me_{eq}	73.8°
Zr-Me_{eq}	2.324Å	N-Zr-Cp(1)	94.4°
Zr-Cp(1)	2.244Å	N-Zr-Cp(2)	94.5°
Zr-Cp(2)	2.243Å	Cl_{ax}-Zr-Me_{eq}	76.2°
		Cl_{ax}-Zr-Cp(1)	97.4°
		Cl_{ax}-Zr-Cp(2)	97.6°
		Me_{eq}-Zr-Cp(1)	113.9°
		Me_{eq}-Zr-Cp(2)	113.3°
		Cp(1)-Zr-Cp(2)	132.5°

Figure 2. Computed structures of $LZrCl_2$ (**1**) and of the LZr(Me)Cl isomers **6a** and **6b**. Cp(1) and Cp(2) represent the cyclopentadienyl centroids.

number. The PM3 semiempirical model utilizes new transition-metal parametrizations implemented in the 4.0 version of the SPARTAN program.[32] In order to test the validity of the parametrizations for Zr, the optimized structure of **2** is compared with the experimental structure from X-ray analysis (Figure 1). Figure 1 gives the bond lengths around Zr (with pyridine N, the α-carbon atoms of the *n*-Bu chains, and the centroids of the Cp rings) and the corresponding bond angles. It is noteworthy that the bond length differences are within 0.05 Å, while the bond angle differences are below 6°.

Both the X-ray crystal structure and the optimized structure of **2** reveal a distorted-trigonal-bipyramidal arrangement around the zirconium atom, with the pyridine and one *n*-Bu group having approximately axial orientations. The most remarkable feature in both structures is the magnitude of the $N-Zr-C_\alpha(Bu_{ax})$ angle: the angle, measured from the side opposite to the $N-Zr-C_\alpha(Bu_{eq})$ bond, is obtuse, amounting to 210.7° in the X-ray structure and to 205.4° in the computed structure.

The comparison of the X-ray and computed structures of **2** lends credence to the notion that also the computed structures of *ansa*-zirconocenes **1** and **3**−**7** are reliable. For zirconocenes **5**−**7** two isomeric structures have been calculated, with equatorial (**5a**−**7a**) and axial chlorine atoms (**5b**−**7b**). In all cases the structures with Cl_{eq} appear to be more stable. These are also the structures of the only isomers that could be isolated from the monoalkylation reactions of **1**, as determined by NMR spectroscopy. For the sake of the following discussion, the computed structures of $LZrCl_2$ (**1**) and the monomethyl, monochloro isomers **6a** and **6b** are shown in Figure 2 with the bond distances and bond angles around the Zr atom.

NMR Characterization of the Species 1−7. Tables 2 and 3 show the ^1H and ^{13}C NMR data of complexes **1**−**7**, together with the assignments as obtained by NOE differential spectroscopy (NOEDS)[33] and heterocorrelated HMQC[34,35] and HMBC[35,36] spectroscopies.

The semiquantitative measurements of the proton dipolar interactions performed by means of NOEDS have been decisive for the determination of the molecular structure of the complexes in solution and for the resonance assignments. The proton and carbon numbering adopted in this discussion is given in Figure 1. Typical NOEDS experiments for $LZr(n\text{-}Bu)_2$ (**2**) are shown in Figure 3.

$LZrCl_2$ (1). The computed structure displays a C_s symmetry, with the pentacoordinated Zr atom in a distorted-trigonal-bipyramidal geometry. One chlorine atom and pyridine are in the axial orientation, while the other chlorine atom and the two Cp rings are in the equatorial orientation. The most remarkable feature is the angle of 212.7° between the Zr atom and the two axial groups, as measured from the side opposite to the equatorial chlorine atom.

The computed features fully agree with the analysis of the ^1H and ^{13}C NMR spectra. Because of the C_s symmetry, the methylenic and Cp rings are equivalent, but because of the nonequivalence of the two chlorine atoms, the methylenic protons and the protons and the carbons of the Cp groups can be differentiated.

$LZr(n\text{-}Bu)_2$ (2). The X-ray structure of $LZr(n\text{-}Bu)_2$, shown in Figure 1, reveals a distorted-trigonal-bipyramidal arrangement around zirconium, with the pyridine and one *n*-butyl substituent having an approximately axial orientation. The deviations from a pure trigonal-bipyramidal arrangement are associated with the axial *n*-Bu substituent: by referring to the numbers in Figure

(33) Neuhaus, D.; Williamson, M. *The Nuclear Overhauser Effect in Structural and Conformational Analysis*; VCH: New York 1989.
(34) Bax, A.; Griggey, R. H.; Hawhins, B. L. *J. Magn. Reson.* **1983**, *55*, 301. Bax, A.; Subramanian, S. *J. Magn. Reson.* **1986**, *67*, 565.
(35) Summers, M. F.; Marzilli, L. G.; Bax, A. *J. Am. Chem. Soc.* **1986**, *108*, 4285.
(36) Bax, A.; Summers, M. F. *J. Am. Chem. Soc.* **1986**, *108*, 2093.

Table 2. ^{1}H NMR Data[a] for Compounds 1−4 and 5a−7a

	compd (solvent)						
hydrogen[b]	**1** ($CDCl_3$)	**2** (toluene-d_8)	**3** (benzene-d_6)	**4** (toluene-d_8)	**5a** (benzene-d_6)	**6a** (toluene-d_8)	**7a** (benzene-d_6)
1, 14	6.64 (m)	6.31 (m)	6.43 (m)	6.40 (m)	6.45 (m)	6.26 (m)	6.36 (m)
2, 15	6.57 (m)	6.11 (m)	6.18 (m)	6.57 (m)	6.19 (m)	6.16 (m)	6.68 (m)
3, 16	6.46 (m)	5.44 (m)	5.52 (m)	5.50 (m)	5.33 (m)	5.24 (m)	5.39 (m)
4, 17	5.68 (m)	4.81 (m)	4.92 (m)	4.81 (m)	5.04 (m)	4.97 (m)	5.04 (m)
6′, 12′	4.46 (d, 18.6)	3.49 (d, 18.0)	3.53 (d, 18.0)	3.49 (d, 18.5)	3.47 (d, 17.9)	3.44 (d, 17.8)	3.48 (d, 17.8)
6, 12	4.14 (d)	3.78 (d)	3.77 (d)	3.82 (d)	3.97 (d)	3.90 (d)	3.97 (d)
8, 10	7.18 (d, 7.7)	6.17 (d, 7.6)	6.18 (d, 7.6)	6.19 (d, 7.8)	6.21 (d, 8.0)	6.22 (d, 7.6)	6.24 (d, 7.6)
9	7.67 (t)	6.68 (t, 7.6)	6.68 (t, 7.6)	6.71 (t, 7.8)	6.71 (t, 8.0)	6.72 (t, 7.6)	6.74 (t, 7.6)
18_{ax}		0.55 (m, CH_2)	0.26 (s)	0.32 (s, CH_2)	1.11 (m, CH_2)	0.52 (s, Me)	0.98 (s, CH_2)
18_{eq}		0.10 (m, CH_2)	−0.39 (s)	−0.89 (s, CH_2)			
others		1.58 (m, CH_2)		0.18 (s, Me)	2.14 (m, CH_2)		0.34 (s, Me)
		1.53 (m, CH_2)		0.04 (s, Me)	1.71 (m, CH_2)		
		1.23 (m, CH_2)			1.23 (t, Me)		
		1.18 (m, CH_2)					
		1.11 (t, Me)					
		0.80 (t, Me)					

[a] 400 MHz at 25 °C. [b] Numbering as given in Figure 1. Key: δ in ppm (multiplicity, J (Hz) or assignment); multiplicity, m = multiplet, d = doublet, t = triplet.

Table 3. ^{13}C NMR Data[a] for Compounds 1−4 and 5a−7a

	compd (solvent)						
carbon[b]	**1** ($CDCl_3$)	**2** (toluene-d_8)	**3** (benzene-d_6)	**4** (toluene-d_8)	**5a** (benzene-d_6)	**6a** (toluene-d_8)	**7a** (benzene-d_6)
1, 14	126.70	112.69	112.96	116.68	115.07	115.75	115.43
2, 15	116.38	117.12	116.62	115.91	118.28	118.75	116.92
3, 16	110.36	107.64	107.79	108.30	108.30	107.85	108.16
4, 17	100.84	98.27	97.35	100.35	99.93	99.50	100.74
5, 13	133.42	126.84	126.75	128.23	129.79	n.d.	129.28
6, 12	36.86	36.65	36.59	36.57	36.61	36.65	36.65
7, 11	162.41	162.07	162.10	160.30	162.26	162.38	161.27
8, 10	122.00	120.46	120.59	120.70	120.81	120.82	120.85
9	138.21	136.53	136.49	136.75	136.67	136.76	136.71
18_{ax}		49.87	30.68	41.21	53.32	33.92	42.90
18_{eq}		41.83	15.37	27.04			
others		37.62		14.14 (Me)	37.33		4.32 (Me)
		36.49		4.42 (Me)	30.86		
		31.33			14.65		
		31.14					
		14.54 (Me)					
		14.08 (Me)					

[a] 100 MHz at 25 °C. [b] Numbering as given in Figure 1. Key: δ in ppm (assignment).

1, the C(18)$_{ax}$−Zr−N angle is 210.7°, and the C(18)$_{ax}$−Zr−C(18)$_{eq}$ angle measures 78.7°. The computationally optimized structure possesses C_s symmetry, with equivalent Cp protons and methylenic residues but nonequivalent protons within each methylenic residue. These features are completely in agreement with the ^{1}H NMR pattern, which displays two methylenic doublets at δ 3.78 and 3.49, four Cp resonances at δ 6.31, 6.11, 5.44, and 4.81, and two distinct series of *n*-Bu resonances.

The methylenic doublets constitute good pivot resonances for the NOE discussion. The PM3 structure reveals that H(6) (pointing toward equatorial *n*-butyl) is farther from the pyridine H(8) than H(6′). The saturation of the H(8) resonance (easily recognized at δ 6.17) enhances the doublet at δ 3.49, thus assigned to H(6′). In turn, the saturation of the latter allows the assignment of the signal at δ 4.81 to the H(4) Cp proton. On the other hand, the saturation of the H(6) doublet at δ 3.78 leads to enhancement of the signal at δ 6.31 (H(1) of Cp) and of H(18)$_{eq}$, the α-methylenic signal of the equatorial *n*-Bu at δ 0.10. The irradiation of H(1) and H(4) allows the unambiguous assignments of the other H(2) and H(3) resonances of Cp at δ 6.11 and δ 5.44, respectively. The assignments determined so far are confirmed by the saturations of H(1) and H(2): the former induces one relevant and one weaker enhancement of the H(18)$_{eq}$ and H(18)$_{ax}$ (at δ 0.55) resonances of the equatorial and axial *n*-Bu groups, respectively; the latter brings about the enhancement of the resonance of H(18)$_{ax}$ only. The irradiation of only the H(1) and H(2) resonances of Cp constitutes a quick and unambiguous method for the structural characterization of this series of complexes.

LZr(Me)$_2$ (3). Although the signals of H(2) and H(8) are coincident in the solvent (benzene-d_6), the irradiation of H(1) and H(2) allows an unambiguous assignment of the methyl resonances. The irradiation of H(2) enhances the methyl resonance at δ 0.26, thus attributed to the H(18)$_{ax}$ protons of axial methyl. The irradiation of H(6) brings about a relevant enhancement of the resonance of the H(18)$_{eq}$ equatorial methyl protons at δ −0.39 and a smaller one of the H(18)$_{ax}$ protons.

LZr(CH$_2$SiMe$_3$)$_2$ (4). By making the same sequential saturation of the signals of H(1) and H(2), it has been possible to assign the methylenic H(18)$_{ax}$ and H(18)$_{eq}$ signals at δ 0.32 and δ −0.89, respectively.

LZr(*n*-Bu)$_{ax}$Cl$_{eq}$ (5a). The methylenic signals at δ 1.11 and 2.14 are relevantly enhanced when the H(2) resonance of Cp at δ 6.19 is saturated, while no or very small enhancements are observed upon irradiation of the H(1) resonance at δ 6.45. The complex is then the isomer **5a**, having axial *n*-Bu and equatorial chlorine. The comparison of the computed energies of **5a** and **5b**

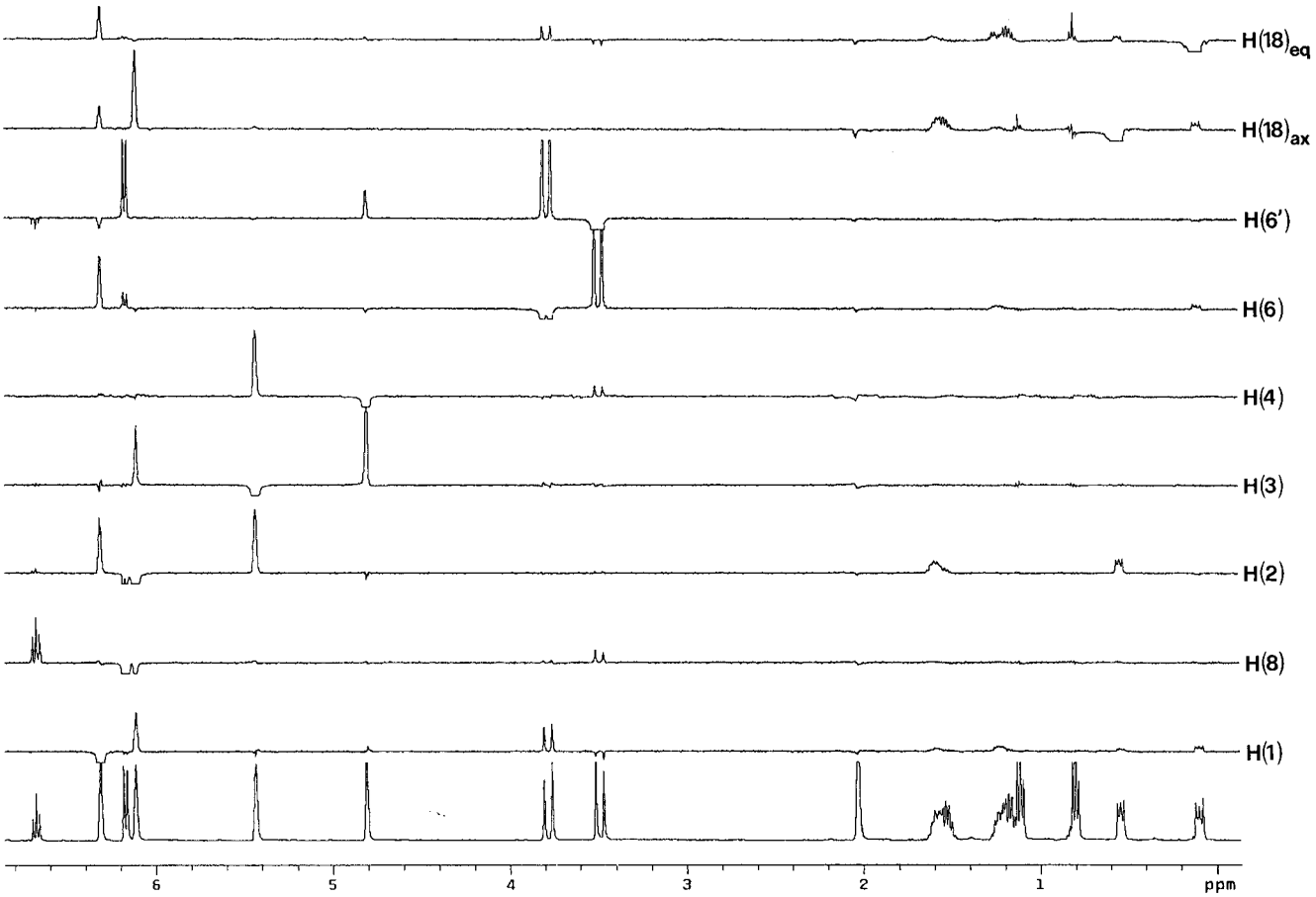

Figure 3. NOEDS spectra of LZr(*n*-Bu)$_2$ (**2**): (bottom trace) unperturbed spectrum; (other traces) differential spectra.

(Table 3) shows that the thermodynamically more stable isomer has actually been isolated. The assignment of the four multiplets of the axial *n*-butyl group was made by their sequential saturation.

LZr(Me)$_{ax}$Cl$_{eq}$ (6a). The methyl signal at δ 0.52 is enhanced when the H(2) resonance of Cp at δ 6.16 is irradiated, while no enhancement is observed upon irradiation of the H(1) resonance at δ 6.26. Both isomers have been computationally investigated at the PM3 level, with full geometrical optimization. The complex with equatorial chlorine is more stable than the isomer with axial chlorine by 1.53 kcal mol^{-1}. The energies have been recalculated on these geometries at the ab initio 3-21G* level. The isomer with the equatorial chlorine is now computed to be more stable, by 4.71 kcal mol^{-1}. Thus it appears that we could isolate the thermodynamically more stable isomer.

LZr(CH$_2$SiMe$_3$)$_{ax}$Cl$_{eq}$ (7a). The irradiation of the H(2) resonance of Cp at δ 6.68 brings about relevant enhancements of methylene and methyl signals of the CH_2SiMe_3 group. Only a smaller enhancement of the methylene group, and none of the methyl group, is observed from saturation of H(1) at δ 6.36. Thus, the complex has the structure given by **7a** with axial (trimethylsilyl)methyl and equatorial chlorine substituents.

Mass Spectrometry. The mass data indicate that the complexes (**2**−**7**) are monomeric, at least in the gas phase. The nature of the various fragments has been confirmed by comparison of experimental and calculated clusters. In the case of the dialkyl derivatives the most abundant fragments correspond to the loss of the two alkyl groups, as expected, except for the complex **3**, where the most abundant fragment is $M^{\bullet+} - CH_3$. Complexes **5**−**7** show $M^{\bullet+} - R$ as the most abundant fragment, in agreement with the stronger Zr−Cl bond as compared with Zr−C$_{alkyl}$ bond.

X-ray Crystal Structure of LZr(*n*-Bu)$_2$ (2). The experimental data of the crystal structure determination are listed in Table 4. Selected bond lengths and angles for the non-H atoms are given in Table 5 and in the Supporting Information.

There are two independent molecules, A and B, in the asymmetric unit with different *n*-butyl group conformations. For the molecule A (Figure 4) the non-H atoms were refined anisotropically, while for the B molecule the butyl groups indicate a systematic conformational disorder with 50:50 population of every part, caused by mirror plane symmetry. An ORTEP view of molecule A, together with the atom-labeling scheme, is given in Figure 4. Molecule B possesses a mirror plane so that the butyl groups are completely disordered with 50:50 occupations caused by symmetry. Thus, it is impossible to determine the relative orientation of the butyl groups in the molecule. The data reported in Table 5 and discussed in connection with the calculated structure refer to molecule A.

In both molecules A and B the plane containing the two α-butyl carbon atoms together with the N pyridine and Zr atoms is almost symmetrically inserted between the two cyclopentadienyl rings. Among the possible coordination modes for 5-coordinated complexes, the molecular configuration seems to be intermediate between a square-pyramidal and a trigonal-bipyramidal

Table 4. Crystal Data and Structure Refinement Details for 2

identification code	gino3
empirical formula	$C_{25}H_{33}NZr$
fw	438.74
habit, color	yellow plate
cryst size	0.10 × 0.08 × 0.02 mm
temp	223(2) K
wavelength (Cu Kα)	1.541 78 Å
cryst syst	orthorhombic
space group	$Cmc2_1$ (No. 36), $Z = 12$
unit cell dimens[a]	$a = 26.629(2)$ Å
	$b = 15.720(1)$ Å
	$c = 15.797(1)$ Å
V	6612.7(8) Å^3
density (calcd)	1.322 g/cm^3
abs coeff	4.127 mm^{-1}
$F(000)$	2760
diffractometer	Enraf-Nonius CAD4
Q range for data collection	3.26−60.01°
index ranges	$-29 \le h \le 0$, $-17 \le k \le 0$, $-17 \le l \le 0$
	$0 \le h \ge 29$, $0 \le k \le 17$, $0 \le l' \le 17$
scan mode	$\omega/2\theta$ scans
scan width	0.94 + 0.51tgq (deg)
no. of rflns collected	3883
no. of indep rflns	3773 (R(int) = 0.0329)
no. of obsd rflns	3268 ($I > 2\sigma(I)$)
intensity and orientation control	3 rflns every 100, 10% linear decay
abs cor	empirical
max and min transmissn	1.000 and 0.257
refinement method	full-matrix least-squares on F^2
no. of data/restraints/params	3773/1/363
goodness-of-fit on F^2	1.070
final R indices ($I > 2\sigma(I)$)[b]	R1 = 0.0460, wR2 = 0.1169
R indices (all data)	R1 = 0.0662, wR2 = 0.1267
abs structure param	0.00(2)
extinction coeff[c]	0.00004(2)
largest diff peak and hole	0.768 and −0.663 e/A^3

[a] From 19 well-centered reflections $41 < \theta < 46.5°$. [b] $R1 = \sum||F_o| - |F_c||/\sum|F_o|$; $wR2 = [\sum w(F_o^2 - F_c^2)^2/\sum w(F_o^2)^2]^{1/2}$; $w = [\sigma^2(F_o^2) + 0.0698P)^2 + 32.08P]^{-1}$, $P = (\max(F_o^2,0) + 2F_c^2)/3$. [c] Extinction correction formula $F^*_c = F_c k[(1 + 0.001F_c^2\lambda^3)/(\sin 2\theta)]^{-1/4}$; k = overall scale factor.

Table 5. Selected Bond Lengths (Å) and Angles (deg) for Molecule A of LZr(n-Bu)$_2$ (2)[a]

Zr(1)−C(18)	2.355(9)
Zr(1)−C(22)	2.385(9)
Zr(1)−N(1)	2.531(8)
Zr(1)−Cp(1)	2.235(5)
Zr(1)−Cp(2)	2.230(5)
C(18)−C(19)	1.543(13)
C(19)−C(20)	1.522(13)
C(20)−C(21)	1.51(2)
C(22)−C(23)	1.526(13)
C(23)−C(24)	1.524(13)
C(24)−C(25)	1.48(2)
C(18)−Zr(1)−C(22)	78.7(3)
C(18)−Zr(1)−N(1)	149.3(3)
C(22)−Zr(1)−N(1)	70.8(3)
Cp(1)−Zr(1)−Cp(2)	130.8
Cp(1)−Zr(1)−N(1)	91.5
N(1)−Zr(1)−Cp(2)	93.0
C(18)−Zr(1)−Cp(1)	101.0
C(22)−Zr(1)−Cp(1)	119.3
C(18)−Zr(1)−Cp(2)	99.4
C(22)−Zr(1)−Cp(2)	108.3
C(19)−C(18)−Zr(1)	121.4(6)
C(23)−C(22)−Zr(1)	122.7(6)

[a] Cp is the centroid of the cyclopentadienyl ring. Symmetry transformations used to generate equivalent atoms: (a) $-x + 2$, y, z.

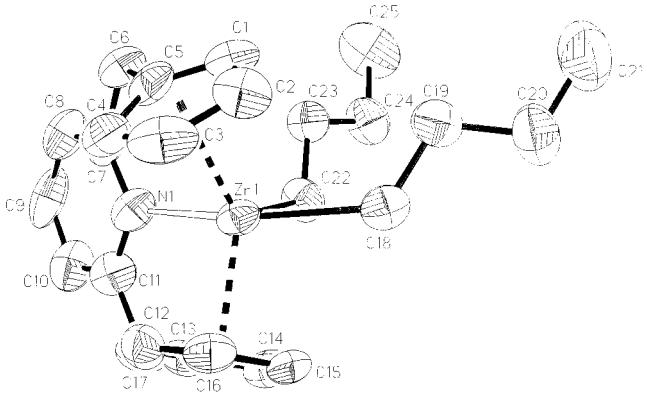

Figure 4. ORTEP view of LZr(n-Bu)$_2$ (**2**) (molecule A).

(tbp) geometry, the latter being somewhat more realistic. In this tbp geometry, the pair of atoms N and C(18) would occupy axial positions, while the two Cp ring centroids and C(22) would lie in the equatorial sites. Comparison of the angles around the zirconium atom reveals that the N−Zr−C(18) (149.3°) axial system is bent toward equatorial C(22). The deviation from linearity is shown by the widening of the angle between the two cyclopentadienyl centroids (Cp(1)−Zr−Cp(2) = 130.8°) and the corresponding reduction of the C(18)−Zr−C(22) angle (78.7°). The Zr−N(pyridine) distance (2.531 Å) is shorter than the analogous Zr−N(pyridine) distance observed in the quite regular tbp complex [{η^5:η^1:η^5:η^1-Et$_8$(C_4H_2N)$_3$(C_5H_3N)Zr=O}$_2$(μ-K)$_2$][37] but longer than the Zr−N(pyridine) distance in non-tbp complexes.[38]

(37) Jacoby, D.; Floriani, C.; Chiesi-Villa, A.; Rizzoli, C. *J. Am. Chem. Soc.* **1993**, *115*, 7025.
(38) Howard, W. A.; Waters, M.; Parkin, G. *J. Am. Chem. Soc.* **1993**, *115*, 4917.

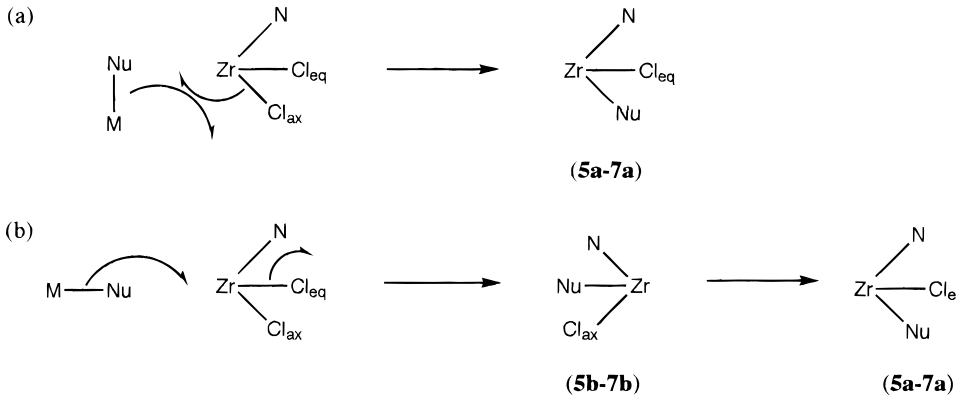

Figure 5. Possible mechanisms of the monoalkylation reaction of $LZrCl_2$: (a) four-center mechanism; (b) nucleophilic substitution mechanism.

Discussion

The different reactivities toward alkylation by nucleophilic substitution of $LZrCl_2$ and Cp_2ZrCl_2 deserve some discussion.

The reaction of Cp_2ZrCl_2 with alkyl Grignard reagents or alkyllithium reagents mainly leads to doubly alkylated products, while the monoalkylated products can be better obtained by alternative routes. At variance, as we show in this paper, monoalkylated products and dialkylated products are easily obtained from $LZrCl_2$ by simply using the appropriate molecular ratios. It is clear that in the case of the Cp_2ZrCl_2 complex the two chlorine atoms display similar reactivities and that the reactivity of the monoalkyl monochloro derivative is about identical with that of the starting dichloro derivative. On the other hand, it may be presumed that the different orientations of axial and equatorial chlorine atoms in trigonal-bipyramidal $LZrCl_2$ makes the reactivity of the two chlorine atoms very different. It may also be suggested that the different reactivities are determined by the different energies of the $Zr-Cl_{ax}$ and $Zr-Cl_{eq}$ bonds, as related to the different bond lengths, although this difference is negligible in the computed model ($Zr-Cl_{ax} = 2.51$ Å, $Zr-Cl_{eq} = 2.48$ Å).

On the other hand, a closer inspection of the PM3-optimized geometry of $LZrCl_2$ shows that the $Zr-Cl_{ax}$ and $Zr-Cl_{eq}$ bonds offer a different hindrance to the approaching nucleophile. While the $Zr-Cl_{eq}$ bond is protected by axial pyridine and axial chlorine groups (as shown in Figure 2, the $N-Zr-Cl_{ax}$ and $Cl_{ax}-Zr-Cl_{eq}$ angles are 70.4 and 77.0°, respectively), the $Zr-Cl_{ax}$ bond is relatively unhindered by the equatorial Cp rings, also because the $N-Zr-Cl_{ax}$ angle is significantly greater than 180°.

Two different mechanisms can be proposed for the alkyl nucleophile approaching $LZrCl_2$ along the back side to the $Zr-Cl_{eq}$ bond.

(i) In the four-center mechanism (Figure 5a) the Cl_{ax} atom is substituted, with direct generation of the isomer (**5a**−**7a**) which has actually been isolated.

(ii) In the nucleophilic substitution mechanism (Figure 5b), the Cl_{eq} atom is substituted. The less stable isomer (**5b**−**7b**) is formed initially, which then will convert to the most stable and isolated isomer (**5a**−**7a**).[39] The observation that the monoalkylated zirconocenes (**5a**−**7a**), with equatorial chlorine, are more resistant to further alkylation would suggest that the four-center mechanism is the working mechanism.

Experimental Section

All reactions were carried out in an atmosphere-controlled (N_2; <1 ppm O_2 and <1 ppm H_2O) automatic glovebox, MBRAUN Model 200 GI, equipped with an internal refrigerator and an apparatus for carrying out reactions at low and high temperatures. All chemicals were reagent grade and were purified as required. Tetrahydrofuran, diethyl ether, and aromatic and aliphatic hydrocarbons were first dried by distillation from $LiAlH_4$ and then from potassium−benzophenone ketyl. Dichloromethane was dried by distillation from calcium hydride. The NMR spectra were recorded on a Varian Unity 400 spectrometer. Deuterated solvents (Cambridge Isotope Laboratories) were dried by sodium−potassium alloy inside the glovebox. Mass spectra were recorded on a VG Organic Ltd. ZAB 2F. Elemental analyses were determined by the microanalytical laboratory of the Department of Chemistry (Perkin-Elmer 240B microanalyzer). The mass spectra of compounds **3**−**7** were recorded with a T_{probe} of 200 °C, while for compound **2** the T_{probe} used was 120 °C, in order to avoid decomposition of the compound before entering into the ionization cell. The main fragmentation patterns have been obtained on the basis of B/E-linked scans.

The NOE spectra have been obtained in the differential mode (NOEDS)[33] on a Varian Unity 400 spectrometer. The lines of the selected multiplet were 0.05 s cyclically saturated for a total time of 10 s with the proper attenuation of the decoupling power.[40] The heterocorrelated reverse-mode HMQC[34,35] and HMBC[35,36] (multiple bond HMQC) spectra have been acquired on the same spectrometer. In a typical experiment, a total of 256 t1 measurements were made in the phase-sensitive acquisition mode, with 16 (HMQC) or 32 (HMBC) scans for t1 value. The delay of the BIRD filter is matched to the average $^1J_{CH} = 140$ Hz. The fixed delay for the detection of multiple-bond correlations is tuned to $^nJ_{CH} = 5$ Hz.

$LZrCl_2$ (1). To a cold solution (−20 °C) of $ZrCl_4$ (2.33 g, 1 mmol) in THF (100 mL) was slowly added a solution (2.79 g, 1 mmol) of the ligand $[2,6\text{-}C_5H_3N(CH_2C_5H_4)_2]^{2-}Na^+_2$, prepared as previously reported,[26] in THF (100 mL) with magnetic stirring at room temperature. After 24 h, the reaction mixture was filtered and washed with THF (3 portions of 10 mL). The

(39) The easy interconversion between dialkylated zirconocenes with different alkyls, $LZr(Me)_{eq}(n\text{-}Bu)_{ax}$ and $LZr(Me)_{ax}(n\text{-}Bu)_{eq}$, has been observed: Paolucci, G.; Zanon, J.; Lucchini, V. Manuscript in preparation. Preliminary results on the ethene polymerization catalyzed by these complexes have shown an increasing reactivity as follows: $LZrR_2 > LZr(Cl)R > LZrCl_2$.

(40) Kinns, M.; Sanders, J. K. M. *J. Magn. Reson.* **1984**, *56*, 518.

pale yellow filtrates were concentrated under vacuum, and *n*-hexane was added. The clear solution was mantained at −30 °C in the refrigerator. A pale yellow precipitate formed after 12 h, which was collected by filtation, washed with *n*-hexane, and dried. Yield: 3.127 g, 76%. Anal. Calcd for $C_{17}H_{15}NCl_2Zr$: C, 51.7; H, 3.8; N, 3.5; Cl, 17.9. Found: C, 52.5; H, 3.9; N, 3.4; Cl, 17.4.

LZr(*n*-Bu)$_2$ (2). To a cooled (−80 °C) suspension of $LZrCl_2$ (0.574 g, 1.453 mmol) in Et_2O (30 mL) was slowly added a diethyl ether solution of 1.2 M *n*-BuMgCl (2.42 mL, 2.906 mmol) diluted with 20 mL Et_2O, with vigorous stirring. At the end the temperature was slowly increased to 0 °C over 2 h and the mixture was stirred at this temperature for 90 min. At 0 °C the color of the mixture changed from light yellow to green-brown. The temperature was increased to room temperature and mantained at this temperature overnight. The solvent was then removed under reduced pressure, and the solid residue was extracted with three portions (50 mL each) of *n*-pentane. The light green solution was concentrated to a small volume (5 mL), and after cooling (−20 °C) for 1 day light green microcrystals were obtained (0.504 g, 80% yield): mp 105−107 °C; dec pt >140−150 °C. Mass spectrometric data (EI, 70 eV, T_{probe} 120 °C (relative intensity, %)): $M^{\bullet+}$, *m*/*z* 437 (2); $M^{\bullet+} - C_4H_9$, *m*/*z* 380 (2); $M^{\bullet+} - 2C_4H_9$, *m*/*z* 323 (100). Anal. Calcd for $C_{25}H_{33}NZr$: C, 68.4; H, 7.6; N, 3.2. Found: C, 67.5; H, 7.9; N, 3.4.

LZrMe$_2$ (3). To a suspension of $LZrCl_2$ (0.670 g, 1.696 mmol) in Et_2O (40 mL) at −60 °C was slowly added a diethyl ether solution of MeLi in Et_2O (0.57 M, 6.0 mL, 3.42 mmol, molar ratio slightly less than 1:2), diluted in 20 mL of Et_2O, with vigorous stirring. At the end of the addition the reaction mixture was stirred for 1 h at this temperature. The temperature was then increased to −30 °C and maintained for 2 h. Finally the reaction mixture was warmed to room temperature and mantained at this temperature overnight. The solvent was then removed under reduced pressure and the solid residue was extracted with three portions (50 mL each) of *n*-pentane. The yellow-green solution was reduced to small volume and after cooling to −30 °C for 1 day, yellow-green microcrystals were obtained (0.271 g, 45% yield). Mass spectrometric data (EI, 70 eV, T_{probe} 200 °C (relative intensity, %)): $M^{\bullet+}$, *m*/*z* 353 (2); $M^{\bullet+} - CH_3$, *m*/*z* 338 (100); $M^{\bullet+} - 2CH_3$, *m*/*z* 323 (95). Anal. Calcd for $C_{19}H_{21}NZr$: C, 64.4; H, 6.0; N, 3.9. Found: C, 64.0; H, 6.5; N, 4.0.

LZr(CH$_2$SiMe$_3$)$_2$ (4). To a suspension of $LZrCl_2$ (0.540 g, 1.37 mmol) in *n*-pentane (40 mL) at −50 °C was slowly added a diethyl ether solution of Me_3SiCH_2Li in Et_2O (0.53 M, 5.17 mL, 2.74 mmol), diluted in 30 mL of *n*-pentane, with vigorous stirring. At the end of the addition the temperature was increased slowly to 0 °C and maintained for 2 h. The color of the solution changed from yellow to deep red. Finally, the reaction mixture was left at room temperature overnight. The reaction mixture was filtered, and the gray-brown solid was washed several times with *n*-pentane and the washing solvent added to the filtrate. The deep red solution was then concentrated to a small volume (about 3 mL) and cooled to −30 °C for 1 day; light yellow microcrystals were obtained (0.294 g, 43% yield). Mass spectrometric data (EI, 70 eV, T_{probe} 200 °C (relative intensity, %)): $M^{\bullet+}$, *m*/*z* 497 (2); $M^{\bullet+} - CH_2SiMe_3$, *m*/*z* 410 (31); $M^{\bullet+} - 2CH_2SiMe_3$, *m*/*z* 323 (100). Anal. Calcd for $C_{25}H_{37}NSi_2Zr$: C, 60.2; H, 7.5; N, 2.8; Si, 11.3. Found: C, 59.5; H, 7.0; N, 3.0; Si, 11.0.

LZr(*n*-Bu)Cl (5). To a solution of $LZrCl_2$ (0.727 g, 1.839 mmol) in THF (20 mL) at −35 °C was slowly added a THF solution of *n*-BuMgCl in THF (1.44 M, 1.25 mL, 1.805 mmol), diluted in 50 mL of THF, with vigorous stirring. At the end of the addition (about 90 min) the reaction mixture was warmed to room temperature and the mixture stirred for 2 days at this temperature. The solvent was then removed from the yellow solution under reduced pressure and the solid residue was washed with five portions (10 mL each) of *n*-pentane to remove the eventually formed dialkyl derivative. The solid residue was extracted with four portions (50 mL each) of toluene. The yellow solution was concentrated under reduced pressure, and after it was cooled to −30 °C for 1 day, a yellow solid was obtained (0.475 g, 62% yield). Mass spectrometric data (EI, 70 eV, T_{probe} 200 °C (relative intensity, %)): $M^{\bullet+}$, *m*/*z* 415 (16); $M^{\bullet+} - C_4H_9$, *m*/*z* 358 (100). Anal. Calcd for $C_{21}H_{24}NZrCl$: C, 60.5; H, 5.8; N, 3.4; Cl, 8.5. Found: C, 61.0; H, 5.5; N, 4.0; Cl, 8.0.

LZr(Me)Cl (6). To a suspension of $LZrCl_2$ (0.79 g, 2.0 mmol) in Et_2O (40 mL) at −60 °C was slowly added a diethyl ether solution of MeLi in Et_2O (0.57 M, 3.5 mL, 1.99 mmol), diluted in 50 mL of Et_2O, with vigorous stirring. The reaction mixture was then mantained for 1 h at this temperature. During this time the color changes from yellow to red. The reaction mixture was then warmed to −30 °C, and this temperature was maintained for 2 h; finally the temperature was increased to room temperature and mantained overnight. The solvent was then removed from the red solution under vacuum and the solid residue was first washed with *n*-pentane (5 portions of 10 mL each) and then extracted with three portions (50 mL each) of toluene. To the solution was added *n*-hexane at room temperature, and the solution was cooled to −30 °C for 1 day, giving a light yellow powder (0.307 g, 41% yield). By recrystallization from benzene light yellow microcrystals were obtained. Mass spectrometric data (EI, 70 eV, T_{probe} 200 °C (relative intensity, %)): $M^{\bullet+}$, *m*/*z* 373 (2); $M^{\bullet+} - CH_3$, *m*/*z* 358 (100). Anal. Calcd for $C_{18}H_{18}NZrCl$: C, 57.7; H, 4.8; N, 3.7; Cl, 9.5. Found: C, 57.1; H, 5.1; N, 4.1; Cl, 8.9.

LZr(CH$_2$SiMe$_3$)Cl (7). To a solution of $LZrCl_2$ (1.062 g, 2.69 mmol) in THF (50 mL) at −40 °C was slowly added a solution of Me_3SiCH_2MgCl in Et_2O (0.96 M, 2.8 mL, 2.68 mmol), diluted in 50 mL of THF, with vigorous stirring. At the end the reaction mixture was slowly warmed to room temperature and left overnight at this temperature and then for 2 h at 40 °C. The solvent was then removed from the yellow-brown solution under vacuum, and the solid residue was washed with five portions (10 mL each) of *n*-pentane. The yellow residue was extracted with four portions (50 mL each) of toluene. By addition of *n*-pentane to the toluene solution a light yellow precipitate was obtained (0.734 g, 61% yield). Mass spectrometric data (EI, 70 eV, T_{probe} 200 °C (relative intensity, %)): $M^{\bullet+}$, *m*/*z* 445 (6); $M^{\bullet+} - CH_2SiMe_3$, *m*/*z* 358 (100). Anal. Calcd for $C_{21}H_{26}NSiZrCl$: C, 56.4; H, 5.9; N, 3.1; Si, 6.3; Cl, 8.0. Found: C, 57.0; H, 6.0; N, 3.3; Si, 6.6; Cl, 7.7.

X-ray Measurements and Structure Determination of LZr(*n*-Bu)$_2$ (2). Single crystals of **2** were obtained by crystallization from *n*-pentane at −30 °C. The crystals were mounted on glass capillaries and centered on a four-circle Enraf-Nonius CAD4 diffractometer.

Three different studies on three different crystals were carried out. A data collection, performed using Mo Kα radiation, has shown that, due to the small size of the crystals ($0.10 \times 0.08 \times 0.02$ mm^3), no intense diffraction data could be collected. While the crystal structure solution and refinement could proceed easily, the absolute structure in the noncentrosymmetric space group $Cmc2_1$ could not be determined reliably. Therefore, an intensity data collection was performed twice using Cu Kα radiation: the first case was carried out without collection of Friedel's opposite reflections but with measurement of systematic absences for a *C*-centered lattice type in order to confirm the correct estimation of the crystal class and lattice. The second measurement with collection of Friedel's opposites was the final one.

Crystal data are summarized in Table 4; selected bond lengths and angles are listed in Table 5. Three intensity standards were measured every 60 min, and a linear intensity decay of ca. 10% was detected over the whole period of the experiment. The data were corrected for Lorenz and polariza-

tion effects and scaled on the intensity standards using the XCAD4 program.[41] Additionally, an absorption correction was applied.[42]

The structure could be solved either by the heavy-atom method using SHELXS-86 program[43] or by direct methods with SHELXTL-5.0.[44] The structure was refined by a full-matrix least-squares procedure against F^2 using SHELXL-93.[45] There are two independent molecules in the asymmetric unit with different butyl group conformations. For the first one all non-hydrogen atoms were refined anisotropically. In the second molecule the butyl groups indicate a systematic conformational disorder with 50% population of every part. The carbon atoms of these butyl groups as well as the C(34) atom of the pyridine ring were refined isotropically; the remaining non-hydrogen atoms were refined anisotropically. All hydrogen atoms were included on the calculated positions with $d(C-H) = 0.97$ Å and $U_{iso} = 0.08$ Å^2. The refinement of 363 parameters led to the following final residuals: R1 = 0.046 and wR2 = 0.1267.

(41) Harms, K. XCAD4, Program for Data Reduction; University of Marburg, Marburg, Germany, 1993.
(42) Walker, N.; Stuart, D. *Acta Crystallogr., Sect. A* **1983**, *38*, 158.
(43) Sheldrick, G. M. SHELXS-86, Program for Crystal Structure Solution; University of Göttingen, Göttingen, Germany, 1986.
(44) SHELXTL 5.0, Program for Crystal Structure Solution; Siemens Analytical Laboratory, Madison, WI, 1995.
(45) Sheldrick, G. M. SHELXL-93, Program for Crystal Structure Refinement; University of Göttingen, Göttingen, Germany, 1993.

Acknowledgment. We are indebted to the Regione Veneto, Department for Industry and Energy, for financial support in purchasing the Varian Unity 400 spectrometer and the Ministry of University and of Scientific and Technologic Research (MURST) for financial support for this research. We are grateful to Mr. S. Formenti for technical support.

Supporting Information Available: Listings of atomic coordinates, bond lengths and angles, torsional angles, and anisotropic displacement parameters for **2** (33 pages). Ordering information is given on any current masthead page.

OM970311R